GENIORS

Research and Innovation Action (RIA)

This project has received funding from the European Union's Horizon 2020 research and innovation programme under grant agreement No 755171.

Start date : 2017-06-01 Duration : 48 Months
http://geniors.eu/

Report on the development of the different MABB precursor synthesis routes and their contribution on MA homogeneity, dust reduction, lowering sintering temperature

Authors : Dr. Gilles LETURCQ (CEA), LETURCQ G. (CEA)

GENIORS - Contract Number: 755171

Project officer: Roger Garbil

Document title	Report on the development of the different MABB precursor synthesis routes and their contribution on MA homogeneity, dust reduction, lowering sintering temperature
Author(s)	Dr. Gilles LETURCQ, LETURCQ G. (CEA)
Number of pages	19
Document type	Deliverable
Work Package	WP7
Document number	D7.3
Issued by	CEA
Date of completion	2020-12-09 17:33:01
Dissemination level	Public

Summary

In advanced nuclear fuel cycles which intend to manage recycling of the main long-lived radionuclides, such as plutonium and minor actinides (MA: americium, neptunium and curium), the use of mixed-oxide fuels will be required. In the case of plutonium, MOX fuels, composed of uranium?plutonium mixed oxides, are currently used in PWRs (pressurized water reactor), whereas for minor actinides, several types of compounds are being studied. These notably include MA-MOX, MOX fuels containing several percent of minor actinides, or MABB (minor actinide bearing blankets), uranium?minor actinide oxide fuels with up to 20 at.% of one or several minor actinides and dedicated to the periphery of the core. In this context, several processes are being developed to fabricate mixed-oxide fuels complying with irradiation specifications in terms of dimensions, density, open porosity, grain size, homogeneity, etc. Currently, the most common processes, i.e., those employed at an industrial scale, are based on a reactive sintering of single oxide powders and only include dry steps such as milling, grinding and thermal treatments. Besides, these dry steps are generally associated with a major drawback: the formation of large amounts of radioactive dust. In the context of the GEN-IV International Forum, the recycling of the valuable actinides and/or the transmutation of the minor ones has motivated the development of innovative and robust fabrication methods. Among them, oxalic (co-)conversion and weak acid resin synthesis routes were developed to obtain various compositions of highly reactive actinide mixed-oxide precursors. The advantages of such synthesis routes are mainly reduced contamination risk and worker radionuclide exposition by lowering dust generation, improved cationic homogeneity, enhanced microstructural properties (especially homogeneity of pore distribution and grain size) for ceramic fuels and finally a decrease of the temperature sintering limiting volatilization of actinides .

Approval

Date	By
2020-12-09 17:33:34	Dr. Gilles LETURCQ (CEA)
2020-12-09 17:37:33	Dr. Jean-Marc ADNET (CEA)
2020-12-14 12:11:43	Mr. Stéphane BOURG (CEA)

CONTENT

This project has received funding from the EURATOM research and training programme 2014-2018 under grant agreement No 755171. The content of this deliverable reflects only the author's view. The European Commission is not responsible for any use that may be made of the information it contains.

This project has received funding from the EURATOM research and training programme 2014-2018 under grant agreement No 755171. The content of this deliverable reflects only the author's view. The European Commission is not responsible for any use that may be made of the information it contains.

INTRODUCTION

In advanced nuclear fuel cycles which intend to manage recycling of the main long-lived radionuclides, such as plutonium and minor actinides (MA: americium, neptunium and curium), the use of mixed-oxide fuels will be required. In the case of plutonium, MOX fuels, composed of uranium–plutonium mixed oxides, are currently used in PWRs (pressurized water reactor), whereas for minor actinides, several types of fuels are being studied. These notably include MA-MOX, MOX fuels containing several percent of minor actinides [1], or MABB (minor actinide bearing blankets), uranium–minor actinide oxide fuels with up to 20 at.% of one or several minor actinides and dedicated to the periphery of the core [2, 3]. In this context, several processes are being developed to produce mixed-oxide fuels complying with specifications in terms of dimensions, density, open porosity, grain size, homogeneity, etc. [3 – 6]. Currently, the most common processes, i.e., those employed at an industrial scale, are based on a reactive sintering of single oxide powders and only include dry steps such as milling, grinding and thermal treatments. They are particularly suitable for single-oxide fuels, such as UOX (UO2) but, in the case of mixed oxides, such as MOX or MABB fuels, the efficiency of these processes in terms of microstructure (notably the fuel pellet densities) and homogeneity control remains limited [3, 4, 7, 8]. Besides, these dry steps are generally associated with a major drawback: the formation of large amounts of radioactive dust. With the UMACS process, a solution was proposed to overcome limitations in terms of density and homogeneity in MABB fuels [4, 9], but it requires additional steps including a long, thus dust-generating, grinding step and two thermal treatments at high temperatures [4]. In the context of the GEN-IV International Forum [10], the recycling of the valuable actinides and/or the transmutation of the minor ones has motivated the development of innovative and robust synthesis methods. Among them, oxalic (co-)conversion has been developed over several years by CEA and AREVA NC (today ORANO) to obtain various compositions of highly reactive actinide mixed-oxide precursors. The advantages of such a synthesis route are mainly reduced dust generation, improved cationic homogeneity [11 – 13] and enhanced microstructural properties (especially homogeneity of pore distribution and grain size) for ceramic fuels. A fabrication of americium-bearing blanket (AmBB) fuels from $U^{IV}_{1.7}Am^{III}_{0.3}[N_2H_5^+,H_3O^+]_{2.3}(C_2O_4)_5,nH_2O$ oxalate thermally converted into $U_{0.85}Am_{0.15}O_{2\pm\delta}$ oxide powder has been done. The synthesis and characterization of the $U_{0.85}Am_{0.15}O_{2\pm\delta}$ mixed oxide powder is first presented and discussed. Then, densification of a pellet prepared from the co-converted powder is studied by dilatometry and under different conditions. Obtained fuels are compared to those fabricated using the UMACS process including a solid-state synthesis and a similar conventional sintering. If this process offers some advantages, it is, however, also based on the use of powders, which should be avoided when working with highly contaminant materials such as americium. A dust free route involving the handling of americium-containing precursor in the form of millimetric spheres is therefore recommended and led to the development of alternative processes using sol–gel method combined with impregnation [14] or weak acid resin as organic template [15]. This later alternative process, called Calcined Resin Microsphere Pelletization (CRMP) [5, 16], consists in pelletizing and sintering oxide microspheres issued from mineralization of metal-loaded ion exchange resin beads. Tests of the process have been carried out on different metals such as lanthanides and uranium. Influence of heat treatment on the characteristics of cerium oxide microspheres and on the quality of final sintered pellet was studied and dense cerium oxide pellets were produced in improved conditions. Uranium dioxide pellets with different porosity contents were also obtained by mixing U_3O_8 and UO_2 like microspheres in different ratios, pelletizing and sintering [17]. In the present study, the CRMP process is applied to the fabrication of uranium-americium mixed oxide compounds in the form of dense $U_{0.90}Am_{0.1}O_{2\pm\delta}$ pellet.

$U_{0.85}Am_{0.15}O_{2\pm\delta}$ FROM OXALIC CO-CONVERSION ROUTE

POWDER SYNTHESIS

U (+IV) and Am (+III) solutions were prepared separately via dedicated protocols. U (+IV) monometallic nitrate solution was obtained through catalytic reduction of a U (+VI) nitrate solution by H_2 on a Pt/Si backing.

This project has received funding from the EURATOM research and training programme 2014-2018 under grant agreement No 755171. The content of this deliverable reflects only the author's view. The European Commission is not responsible for any use that may be made of the information it contains.

Hydrazinium nitrate ($N_2H_5^+$, NO_3^-) was employed as an anti-nitrous agent to stabilize the (+IV) oxidation state of uranium. Am (+III) nitrate solution was prepared by dissolution of the corresponding oxide powder in concentrated hot nitric acid, with addition of hydrogen peroxide as a catalyzer. Americium oxide dissolution was carried out in a hot cell to limit the exposure of workers to radiation. The cationic concentration of each solution was determined by UV–visible absorption spectroscopy. As-obtained actinide (+III) or (+IV) solutions were mixed together in the desired ratio to achieve the selected cationic stoichiometry in the final oxide. This mixture was prepared as late as possible to avoid radiolysis phenomena. This solution and the precipitation agent, concentrated oxalic acid, were then added simultaneously in a vortex effect reactor. The precipitation occurred in free acid nitric media with an excess of oxalic acid. The oxalate precursor precipitated as soon as the reagents were in contact. From XRD (X-ray diffraction), the obtained solid is a mixed-oxalate phase, $U^{+IV}_{1.7}$ $Am^{+III}_{0.3}$ $[N_2H_5^+, H_3O^+]_{2.3}(C_2O_4)_5$, nH_2O, which has a hexagonal crystalline structure. The latter was already described in a previous work [11]. The crystallized powder was filtered and dried at room temperature, then treated for 3 h at 1023 K under an argon flow to form the required $U_{0.85}Am_{0.15}O_{2\pm\delta}$ oxide.

POWDER CHARACTERIZATION

POWDER COMPOSITION AND RESIDUAL CARBON: TIMS MEASUREMENTS AND TGA-µGC

After powder synthesis, thermal ionization mass spectrometry (TIMS) analyses were performed to assess the final Am/(U + Am) ratio. A VG-54 magnetic sector mass spectrometer was used. The obtained oxide was dissolved in nitric acid and diluted in water. An internal standard of known isotopic composition and concentration was added to the sample. Actinide content was determined and assessed from the measured final sample concentrations and the known internal standard concentration. The Am/(U + Am) ratio found equal to 15.8 ± 0.3 at.% is slightly higher than the target value (15%), but remains in fair agreement with it. The ratio of carbon still remaining in the powder after calcination was estimated by thermogravimetric analysis (TGA) coupled with gas chromatography measurements (lGC). It was found to be equal to 2690 ± 120 ppm. Such high carbon content would presumably be problematic and generate additional porosity during the sintering thermal treatment unless it is properly removed before the densification [18].

XRD ANALYSIS

XRD analysis of the synthesized powder was performed using a D8 Bruker Advance diffractometer especially equipped for radioactive material measurements. For peak position correction, gold powder was added as a 2θ standard. The diffractogram in Fig. 1 shows that a monophasic fluorite-type uranium–americium mixed oxide (space group 225) is present, without any additional phases. Impurities could not be revealed because of the detection limit of XRD. In particular, carbon present in too small quantity or in an amorphous state cannot be observed. A lattice parameter of 5.4615(3) Å was determined from Le Bail refinement using the Fullprof suite [19]. This value is smaller than those typically reported for this composition, i.e., around 5.468 Å [4, 20]. Such a difference, around 0.007 Å, is probably caused by a higher O/M (oxygen to metal) ratio for the co-converted compound. Most of the reported uranium–americium oxide materials were heat-treated at high temperature under reducing atmospheres, inducing lower O/M ratios than for the considered powder, calcinated under argon at a relatively low temperature. From **Figure 1** diffractogram, the mean crystallite size was estimated using the Williamson–Hall plot [21–23] and gives a value of 26 ± 3 nm for the $U_{0.85}Am_{0.15}O_{2\pm\delta}$ powder. From the refined lattice parameter and considering a hypothetical O/M ratio of 2, a $U_{0.85}Am_{0.15}O_2$ theoretical density of 10.993 $g.cm^{-3}$ was established. This value was used to determine densities of the sintered samples.

This project has received funding from the EURATOM research and training programme 2014-2018 under grant agreement No 755171. The content of this deliverable reflects only the author's view. The European Commission is not responsible for any use that may be made of the information it contains.

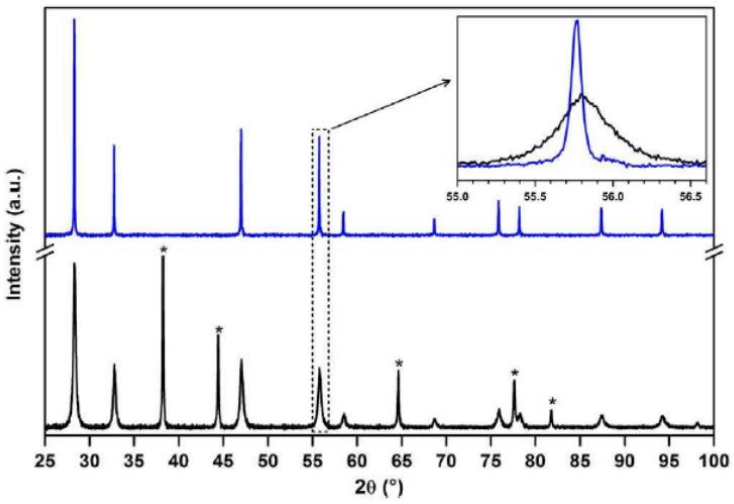

Figure 1. XRD pattern of ground $U_{0.85}Am_{0.15}O_{2\pm\delta}$ (black color) after co-conversion (asterisks indicate Au standard diffraction lines) and (blue color) after sintering for 5 h at 1923 K under Ar/H_2 (4%).

SEM OBSERVATIONS

The powder was characterized using a nuclearized Zeiss SUPRA 55/55VP FEG-SEM (field emission gun scanning electron microscope). SEM micrographs presented in **Figure 2** show a typical morphology for a wet chemical route.

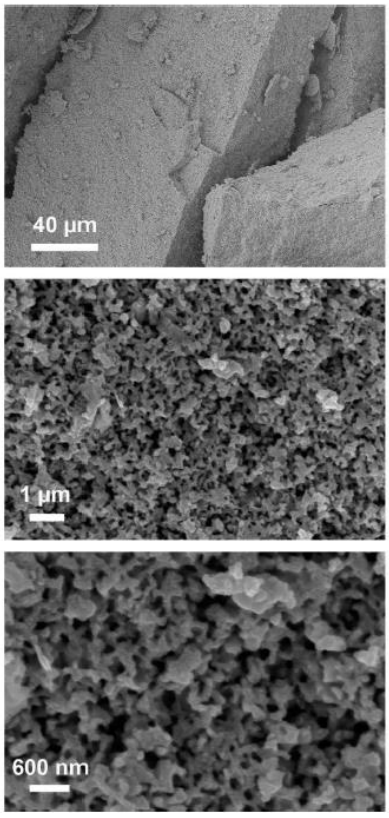

Figure 2. FEG-SEM micrographs of co-converted $U_{0.85}Am_{0.15}O_{2\pm\delta}$ powder in secondary electron mode.

This project has received funding from the EURATOM research and training programme 2014-2018 under grant agreement No 755171. The content of this deliverable reflects only the author's view. The European Commission is not responsible for any use that may be made of the information it contains.

The powder is composed of large agglomerates of several hundred micrometers. These soft and porous agglomerates are composed of submicronic particles, similar to those obtained in AmO_2 powder synthesis [24], which includes precipitation in an aqueous environment followed by a filtration/crushing step. Because of this specific particle size distribution, proper laser granulometric measurements could not be performed.

DENSIFICATION BY SINTERING

PELLETIZING GREEN PELLETS WERE PREPARED FROM THE CO-CONVERTED OXIDE POWDER.

Pelletizing was performed using uniaxial pressing (550 MPa for 10 s) in a 4.9-mm-diameter three-part die. Before adding the powder, the tungsten carbide die was lubricated with a saturated solution of stearic acid in ether. No lubricants or additives were, however, added to the powder. Despite the presence of large agglomerates in the precursor oxide powder, cylindrical green pellets exhibiting neither deformations nor defects were obtained, with a repeatable density of 49 ± 1% TD.

DILATOMETRIC ANALYSIS

Dilatometric measurements were carried out using a horizontal Netzsch DIL 402 C dilatometer integrated in a glove box. Its furnace chamber, sample holder and push rod are made of graphite, but all parts in contact with the samples were tungsten to avoid any reactions between the oxide and the carbon at high temperatures. Extensive specifications are detailed in a previous publication [9]. The pellet linear shrinkage was recorded from RT (room temperature) to 2173 K with a heating rate of 3 K min1 under a constant flow of Ar/H_2 (4%) of 12 L h^{-1}. The relative variation of the sample length (dL/L_0) is reported in Figure 3, which also contains the shrinkage rate, i.e., the derivative of dL/L_0 as a function of time. The graphical plotting of shrinkage rate is convenient for determining the onset temperature of sintering.

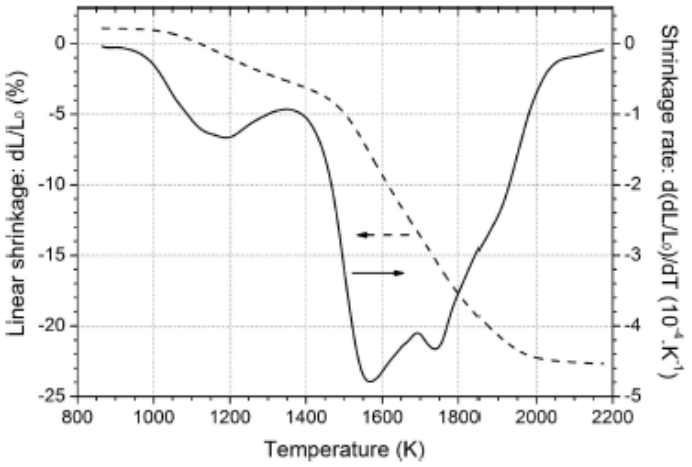

Figure 3. Dilatometric curve and evolution of the shrinkage rate of the co-converted $U_{0.85}Am_{0.15}O_{2\pm\delta}$ compound at 3 K min^{-1} under Ar/H_2 (4%).

For the $U_{0.85}Am_{0.15}O_{2\pm\delta}$ sample, the sintering begins around 800 K. The densification is then slowed down from 1200 till 1350 K, due to a possible additional crystallization or carbon loss. The highest shrinkage rate is reached between 1550 and 1750 K. At higher temperatures, the shrinkage rate progressively decreases and becomes null around 2000 K, indicating the end of sintering. Around 1900 K a change in the slope of the shrinkage rate curve

This project has received funding from the EURATOM research and training programme 2014-2018 under grant agreement No 755171. The content of this deliverable reflects only the author's view. The European Commission is not responsible for any use that may be made of the information it contains.

is observed, which may indicate a change in sintering mechanism around this temperature. With this first sintering cycle performed without any temperature plateaus, a sintered pellet with a density of 94.3 ± 0.5% TD was finally obtained. Due to the fast drop of the shrinkage rate beyond 1900 K, it is not necessary to reach higher temperatures to achieve high densities, however an isothermal plateau might be required.

SINTERING EXPERIMENTS

Thermal treatments for sintering green pellets, coming from co-converted $U_{0.85}Am_{0.15}O_{2\pm\delta}$ powder were selected thanks to data obtained through dilatometric measurement. These sintering processes were carried out in an all-tungsten high-temperature furnace located in a hot cell. The selected process for elaboration of fuel pellets is a "simplified" process composed of only 2 steps: pelletizing and sintering, thus avoiding any grinding/dust generating steps. Three thermal treatments were applied under Ar/H_2 (4%) on pellets with green densities around 50% TD. The cycles only differ in their plateau temperatures:

- A: 293 K – 3 K min^{-1} → 1823 K, 5 h – 3 K min^{-1} → 293 K;
- B: 293 K – 3 K min^{-1} → 1873 K, 5 h – 3 K min^{-1} → 293 K;
- C: 293 K – 3 K min^{-1} → 1923 K, 5 h – 3 K min^{-1} → 293 K.

These sintering processes led to pellets with densities of 93.9 ± 0.5% TD, 94.7 ± 0.5% TD and 95.7 ± 0.5% TD, corresponding to Thermal Treatments A, B and C, respectively. For Cycles B and C, the 5 h plateau allowed reaching higher densities than that of the dilatometric experiment, despite the lower maximum temperature. As densities higher than 94% TD are considered for AmBB compounds **[3, 4, 25]**, only Treatments B and C appeared to give results complying with this requirement. Thus, only pellets sintered at 1923 K during 5 h were further characterized. It is worth noting that even though the oxygen potential varies with temperature, the variation between 1823 and 1923 K is, in such conditions, is very low. The difference in density was thus not caused by the difference in oxygen potential (**Figure 2**).

CHARACTERIZATION OF THE PELLETS SINTERED AT 1923 K FOR 5 H

COMPOSITION AND CARBON RATIO: TIMS MEASUREMENTS AND TGA-µGC

Americium oxides have high oxygen potentials, which induces a significant risk of sublimation that must be taken into account during the high-temperature reducing thermal treatment. TIMS analysis was thus performed on the sintered compound, giving an Am/(U + Am) ratio equal to 15.6 ± 0.2 at.%. This value, similar to that of oxide precursor, indicates that there was no americium sublimation at a significant level during the sintering process. The carbon content of the pellet sintered at 1923 K for 5 h under a reducing atmosphere was measured by TGA-lGC, under air, and found to be 365 ± 120 ppm. A decrease of 86% of the initial carbon content was thus obtained during the thermal treatment. As this result was obtained without any optimization for this parameter, it may be possible to further lower the final carbon content, if necessary.

STRUCTURAL ASPECTS: XRD ANALYSIS

An XRD analysis was conducted on a powdered fragment of the pellet. After sintering, the obtained diagram (**Figure 1**) still corresponds to a sole fluorite-type structure. Within the XRD detection limits, there are thus no additional phases. Besides, a notable improvement of crystallinity is observed, as the diffraction peak FWHM (full-width at half-maximum) are strongly reduced after sintering (**Figure 1**). This is accompanied by an increase of crystallite size of at least 0.1 µm according to the Williamson–Hall plot. The lattice parameter was found to be

This project has received funding from the EURATOM research and training programme 2014-2018 under grant agreement No 755171. The content of this deliverable reflects only the author's view. The European Commission is not responsible for any use that may be made of the information it contains.

equal to 5.4647(1) Å. This post-sintering increase in lattice parameter can be explained by a decrease of the O/M ratio and maybe by the removal of impurities. Concerning the O/M ratio, no attempts were made in this study to control it because of the lack of thermodynamic data for U–Am mixed oxides. It remains worth noting that this parameter could be controlled during the sintering heat treatment by changing the atmosphere, whether during the whole sintering cycle or only the plateau and/or during cooling. Previous studies reported that U–Am mixed-oxide sintering could be performed in various oxygen potentials ranging for instance between 520 and 325 kJ mol^{-1} **[3 4, 26]**.

PELLET PROFILES AND MORPHOLOGIES

Before and after sintering, produced pellets were visually examined, and for all of them, no macroscopic defects were present. The pellet profiles were measured using a laser profilometer **[27]**. As an example, Figure 4 shows the profile of a sintered pellet, representative of the tested samples. The maximum variation of the diameter is inferior to 12 µm. Moreover, no deformations pre- or post-sintering were observed. Fracture surfaces from sintered pellets were examined with a FEG-SEM in order to observe their microstructure. To gain an increased contrast during acquisition, the selected fragment was tilted. The sample fracture mode is here inter-granular. The micrograph in Fig. 5, representative of the overall sample, reveals a dense and homogeneous microstructure, composed of polyhedral grains of about 5–20 µm. Significant grain growth is evidenced by this grain size, compared to that of the initial powder. Only residual and submicronic pores can be observed for this sample. Such microstructural features confirm that the last sintering stage has been reached, in agreement with the sintered density.

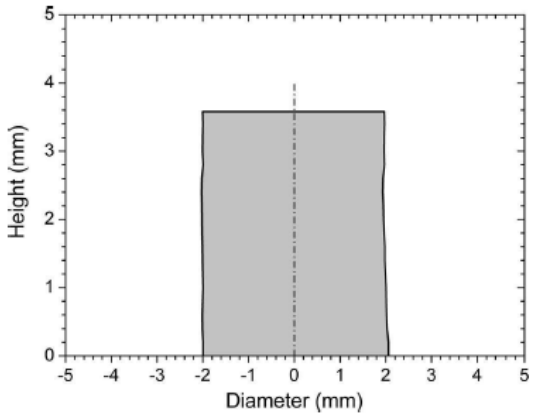

Figure 4. Profile of an $U_{0.85}Am_{0.15}O_{2\pm\delta}$ pellet sintered for 5 h at 1923 K under Ar/H_2 (4%)

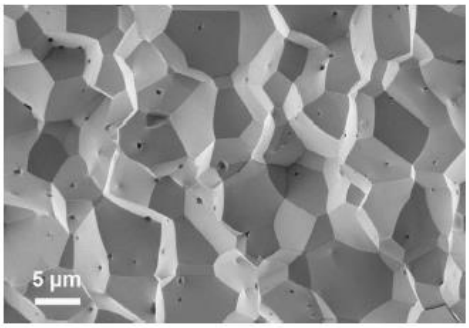

Figure 5. FEG-SEM micrograph in secondary electron mode of the fracture surface of an $U_{0.85}Am_{0.15}O_{2\pm\delta}$ pellet sintered for 5 h at 1923 K under Ar/H2 (4%).

This project has received funding from the EURATOM research and training programme 2014-2018 under grant agreement No 755171. The content of this deliverable reflects only the author's view. The European Commission is not responsible for any use that may be made of the information it contains.

COMPARISON TO ANOTHER FABRICATION PROCESS

In this section, obtained results are compared to those commonly obtained with the UMACS process (Uranium Minor Actinide Conventional Sintering). This powder metallurgy process is used for $U_{1-x}Am_xO_{2\pm\delta}$ dense pellet fabrications from single oxides, and was notably employed for the analytic irradiation program DIAMINO [4]. Its main feature is the synthesis, before the sintering step, of the $U_{1-x}Am_xO_{2\pm\delta}$ compound through a solid-state reaction between single oxides at high temperature, as described in Figure 6.

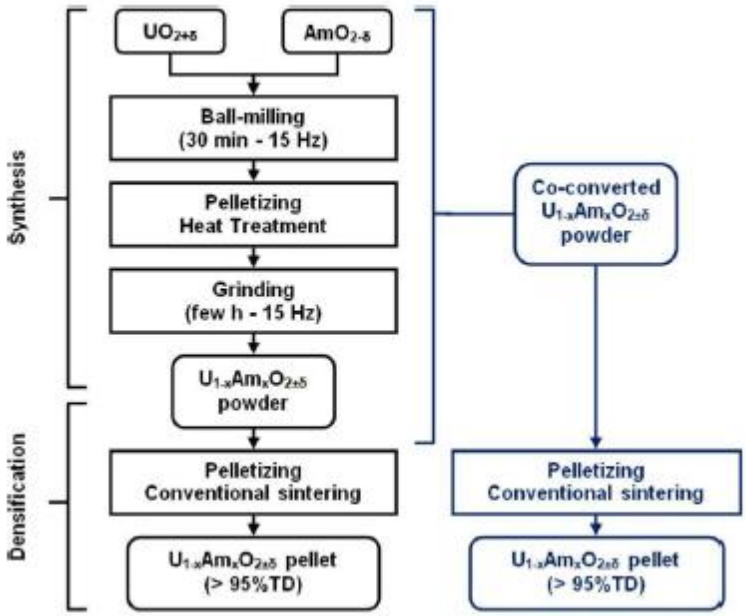

Figure 6. Comparison between the flowcharts of the UMACS process (left) and that based on the use of co-converted powders (right) for $U_{0.85}Am_{0.15}O_{2\pm\delta}$ dense pellet fabrication.

Though this process makes the fabrication of pellets with densities superior to 94% TD possible, there is a major drawback. Two high-temperature treatments are required, as well as an intermediate long grinding step which is responsible for dust generation. On the contrary, the simplified process based on the use of co-converted powder does not need a milling step, which limits dust creation. Another advantage of co-converted powders is the decrease of the required sintering temperature to reach the same target density of 95% TD [4]. For this $U_{0.85}Am_{0.15}O_{2\pm\delta}$ compound, this temperature is at least 100 K lower than that used for the UMACS process. This difference is presumably a result of the high chemical reactivity of the co-converted powders due to the fineness of the powder particles, as evidenced by SEM micrographs in Figure 2 and by the determined mean crystallite size of 26 ± 3 nm (value determined using a modified Thompson Cox Hastings Pseudo Voigt profile function for XRD diagram refinement). In summary, the co-converted route presents several advantages compared to the UMACS route: the simplification of the process through the reduction of the number of steps and the lowering of the sintering temperature and dust production, which could be clinchers for industrialization of this simplified process.

CONCLUSION ON FABRICATION OF $U_{0.85}Am_{0.15}O_{2\pm\delta}$ VIA OXALIC CO-CONVERSION ROUTE

The final goal of this work was to demonstrate the feasibility of the fabrication of $U_{0.85}Am_{0.15}O_{2\pm\delta}$ dense pellets from co-converted powders. Dense pellets with homogeneous composition and microstructure, a low level of

This project has received funding from the EURATOM research and training programme 2014-2018 under grant agreement No 755171. The content of this deliverable reflects only the author's view. The European Commission is not responsible for any use that may be made of the information it contains.

carbon, and a very limited residual porosity were obtained. These pellets were rectilinear, and neither deformations nor particular defects were observed. The selected process for production is a simplified one, with only two steps: pelletizing and sintering. Despite an extensive agglomeration of the particles in the initial powder, no grinding steps were required to reach high densities. This choice makes the reduction of dust production and associated risks possible compared to a conventional method such as the UMACS process. Residual carbon, coming from the initial co-converted oxalate and partially retained after co-conversion (~2700 ppm), was not a limiting factor in obtaining pellets with high densities. Final carbon content in sintered pellets was estimated at around 400 ppm, corresponding to a reduction of 86%. Sintering behavior of the $U_{0.85}Am_{0.15}O_{2\pm\delta}$ co-converted powder was studied under reducing atmosphere by dilatometry. From this study, a 5 h at 1923 K thermal treatment was selected to fabricate pellets. This sintering temperature is 100 K lower than that generally used to sinter the same compound synthesized via solid-state reaction, though both routes give similar results in terms of density and microstructure. This important improvement in AmBB elaboration can be attributed to the high reactivity of the co-converted powders compared to the powders obtained via solid-state reaction. However, despite these advantages, this process is still based on the use of powders which should be avoided when working with highly contaminant materials such as americium. A dust free route involving the handling of americium-containing precursor in the form of millimetric spheres is therefore recommended. The following section exposes work performed to make $U_{0.90}Am_{0.1}O_{2\pm\delta}$ pellet using Calcined Resin Microsphere Pelletization (CRMP) process [5, 16].

$U_{0.9}Am_{0.1}O_{2\pm\delta}$ FROM CRMP PROCESS

Calcined Resin Microsphere Pelletization (CRMP) [5, 16], consists in pelletizing and sintering oxide microspheres issued from mineralization of metal-loaded ion exchange resin beads. Tests of the process have been carried out on different metals such as lanthanides and uranium. Influence of heat treatment on the characteristics of cerium oxide microspheres and on the quality of final sintered pellet was studied and dense cerium oxide pellets were produced in improved conditions. Uranium dioxide pellets with different porosity contents were also obtained by mixing U_3O_8 and UO_2 like microspheres in different ratios, pelletizing and sintering [17]. In the present study, the CRMP process is applied to the fabrication of uranium-americium mixed oxide compounds in the form of dense $U_{0.90}Am_{0.10}O_{2\pm\delta}$ pellet.

SYNTHESIS OF $U_{0.9}Am_{0.1}O_{2\pm\delta}$ MICROSPHERES

EXPERIMENTAL

OXIDE MICROSPHERE SYNTHESIS

RESIN PREPARATION

The ion exchange resin used for the fixation was an IMAC HP333 carboxylic resin supplied by Dow Chemicals (Dow Chemicals, Chauny, France). The resin was sorted beforehand under wet condition and the 630–800 µm size range was selected for experiments. An extensive washing cycle was then performed on the resin (ammonia, nitric acid and demineralised water) in order to remove the synthesis residues and cationic impurities still present. Eventually, the washed resin was prepared in its protonated form.

PREPARATION OF THE LOADING SOLUTION

The loading solution was prepared in two steps. A stock solution of americium (III) nitrate ($Am(NO_3)_3$) was first obtained by the dissolution of 297 mg of AmO_2 powder in a 1 M nitric acid solution. This solution corresponded to a volume of 12.5 mL and to a 0.08 mol L^{-1} Am nitrate solution and to an excess of nitric acid of 0.11 mol L^{-1}.

This project has received funding from the EURATOM research and training programme 2014-2018 under grant agreement No 755171. The content of this deliverable reflects only the author's view. The European Commission is not responsible for any use that may be made of the information it contains.

Then uranium trioxide solid (UO_3) (prepared as in Ref.[15]) was added to this solution as well as deionized water and molar nitric acid. The role of UO_3 dissolution was to increase both pH and uranium concentration by reacting with acid excess and by forming hydrolysed uranyl species. The final solution corresponded to an Acid Deficient Nitrate Uranyle solution (ADUN) [28] mixed to americium nitrate with the following uranium formula $UO_2(NO_3)_{1.2}(OH)_{0.8}$ and with uranium and americium concentrations of 0.101 and 0.012 mol L^{-1}, respectively, an Am over metal ratio of 10.5 at.% and a volume of 83 mL. Characteristics of the resin and initial load used for the fixation are gathered in **Table 1**.

Table 1 Characteristics of the resin and loading solution.

Resin	Dow chemicals H^+ form	IMAC HP333
Loading solution	m (g)	0.904
	Q_{weight} (meq/g)	11.6
	V (mL)	83
	[U] (mmol L^{-1})	101
	[Am] (mmol L^{-1})	11.9
	[Am/(Am + U)] (%)	10.5
	pH	3.93

Q_{weight}: scientific weight capacity in meq/g dry H^+ resin
meq/g dry H^+ :milliequivalent per gram of dry H^+ resin

CATION EXCHANGE

Resin beads were rehydrated and introduced into a glass column. The load solution was recirculated 6 times through the resin bed at a controlled flow rate of 2 mL min^{-1} for a total contact time of 4 h. pH of the load solution was recorded during fixation. From the moment when pH did not change significantly, exchange reaction was considered to be achieved. The loaded resin was then washed with deionized water and drained under low vacuum. The initial load and eluate solution were then analyzed by thermal ionization mass spectrometry (TIMS), in order to determine metal concentrations and to express the fixation yield. The metal loaded resin was then directly heat treated without any more drying.

THERMAL TREATMENTS

A first thermogravimetric analysis (Netzsch STA 449 thermogravimetric analyser) was carried out on a sample of the metal loaded resin under a reconstituted air flow (Airliquide, 20 vol.% O_2–80 vol.% N_2) up to 800 °C. Gas releases (i.e., H_2O, CO_2, CO) were monitored using a coupled gas micro-chromotography module (SRA), (TGA–µGC). Two thermal treatments were then applied to the microsphere lot in a tubular furnace (Lenton LTF). The resin was firstly calcined at 700 °C for 1 h under a reconstituted air flow (10 NL h^{-1}). Initial heating rate of 5 °Cmin^{-1} was reduced to 1 °C min^{-1} from 200 °C up to final temperature in order to ensure an optimal evacuation of the calcination gas generated during the degradation of the polymer and avoid crack formation [5]. The oxide formed at 700 °C was secondly reduced under a reducing treatment in Ar/H_2 (4 vol.%) at 700 °C for 6 h with a constant heating rate of 10 °C min^{-1}.

OXIDE MICROSPHERE CHARACTERIZATION

The crystalline structure of the resulting oxide was characterized by X-ray diffraction (XRD) using a θ–θ D8 advance BRUKER diffractometer equipped with a copper anticathode ($\lambda(K^{Cu}_{\alpha 1})$ = 1.54056 Å, $\lambda(K^{Cu}_{\alpha 2})$ = 1.54439 Å). XRD patterns were collected in presence of an internal Au standard at room temperature by step scanning (0.02° steps at 1 s/step) across the angular range $10° \leq 2\theta \leq 80°$. A Field Emission Gun Scanning Electronic

This project has received funding from the EURATOM research and training programme 2014-2018 under grant agreement No 755171. The content of this deliverable reflects only the author's view. The European Commission is not responsible for any use that may be made of the information it contains.

Microscope (FEG-SEM, Zeiss Supra-55 VP) was used in order to observe the morphology and the microstructure of the synthesized oxide microspheres.
The apparent density of the microspheres was determined by volume and mass measurements of a representative sample of a few hundreds of beads. The number of spheres and the sample volume were obtained from image analysis of one layer of microspheres (assumed as perfect spheres) using an optical microscope (Olympus BX30 M) coupled to an Ellix pattern recognition software (Microvision).
The residual carbon content of the reduced oxide was determined by monitoring the CO_2 emissions occurring during calcination up to 1000 °C under air of the oxide precursors, via TGA–µGC analysis.
The metal contents of the oxide were determined from TIMS analysis of dissolved oxide.

RESULTS AND DISCUSSION

LOADING OF THE RESIN

EXCHANGE EQUILIBRIUM

The different hydroxide complexes of the ADUN solution, mainly $(UO_2)_2(OH)^{3+}$ and $(UO_2)_2(OH)_2^{2+}$, constitutes the driving force of the exchange reaction between the counter-ions H^+ in the resin and UO_2^{2+} and Am^{3+} cations in solution **[7]**. Acting like a buffer, it notably prevents from pH increase caused by the release of H^+ in solution and allows the ion exchange reaction to take place as shown in **Equation 1** in the case of U exchange only (R representing the exchangeable site of the resin):

$$2RH + (UO_2)_2(OH)_2^{2+} + 2NO_3^- \rightarrow R_2(UO_2) + UO_2^{2+} + 2NO_3^- + 2H_2O$$ **Equation 1**

The determinations of Am/(U + Am) ratios in the loading solution (10.5 ± 0.3 at.%) and in the oxide (10.7 ± 0.2 at.%) are not significantly different. Therefore, the resin does not exhibit any selectivity between UO_2^{2+} and Am^{3+} cations at this Am content level.

KINETIC OF THE EXCHANGE REACTION

Evolution of pH in the load solution during exchange (**Figure 7**) describes the exchange kinetics. The pH of the load solution significantly decreases during the first hour and a half when exchange is occurring and then stabilises after 4 h of contact when equilibrium is reached. Exchange is slow because it is mainly governed by interdiffusion of monovalent and divalent/trivalent cations in the resin **[29]** with weak diffusion coefficients (typical values of 8 x 10^{-9} cm^2s^{-1} for trivalent cations and 1.6 x 10^{-7} cm^2s^{-1} for monovalent H^+) and conversion times are about 3 h in this case **[30]**.

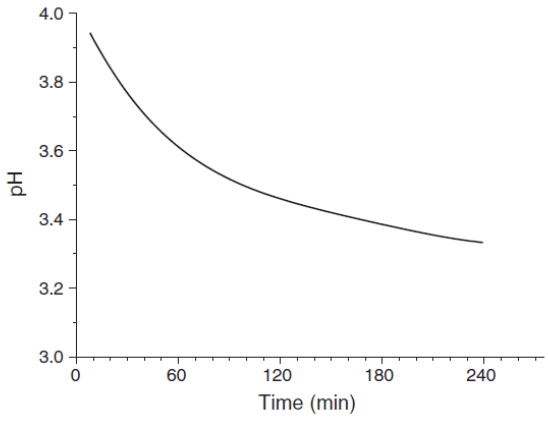

Figure 7 Evolution of pH in the loading solution as a function of time of exchange.

This project has received funding from the EURATOM research and training programme 2014-2018 under grant agreement No 755171. The content of this deliverable reflects only the author's view. The European Commission is not responsible for any use that may be made of the information it contains.

FIXATION YIELD

Fixation yield is calculated from the ratio of the amount of actinide cations fixed in the resin, expressed in meq, over the capacity of the resin used (**Table 2**). Its value equals 66% which is in fair agreement with previous studies concerning the loading of UO_2^{2+} alone which reports a yield fixation of 57% **[16]**. Taking into account Am/(U + Am) ratio in the resin and considering that the resin is exchanged up to 66%, the formulation of the metal loaded resin may be written as:
$R_{21}(UO_2)_9Am;(RH)_{11}$ (with R representing the resin exchangeable site).

Table 2 : Fixation yield of UO22+ and Am3+ in the resin.

n (UO_2^{2+}) loaded (mmol)	3.0
n (Am^{3+}) loaded (mmol)	0.3
Fixed An (meq)	6.9
Resin capacity (meq)	10.4
Fixation yield (%)	66

OXIDE MICROSPHERES SYNTHESIS

THERMOGRAVIMETRIC AND GAS ANALYSIS

Thermogravimetric analysis by TGA–µGC was carried out on the loaded resin and is shown in **Figure 8**. The monitoring of the gas released during calcination in air is reported in **Figure 9**. A first 15.4% weight loss was recorded between 30 °C and 250 °C associated with an endothermic reaction. This phenomenon is attributed to the dehydration of the resin which gives two H_2O emissions peaks revealed by µGC analysis. The peak (a) between 30°C and 70 °C is associated with a mass loss of 3.2% and corresponds to the evacuation of H_2O still present in the resin pores. The peak (b) is recorded between 70 °C and 180 °C with a weight loss of 12.2%. It would correspond to the water of hydration of uranyl(VI) and americium(III) cations bound to the resin **[29]**. The mean hydration number of the actinide cation inside the resin would equal 4.

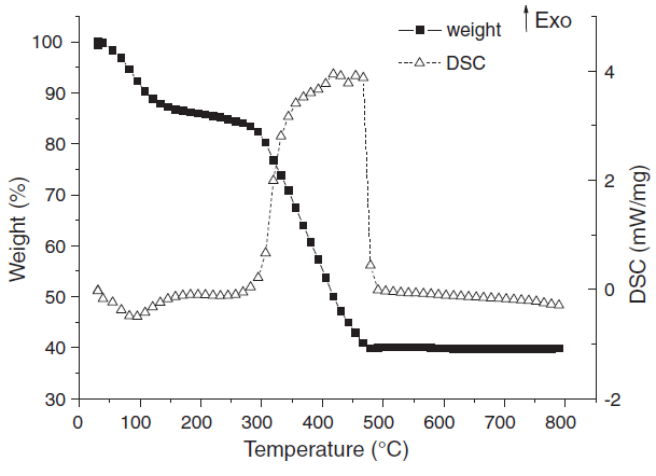

Figure 8 TGA/DSC analysis of the thermal decomposition of UO22+–Am3+ loaded resin in air.

This project has received funding from the EURATOM research and training programme 2014-2018 under grant agreement No 755171. The content of this deliverable reflects only the author's view. The European Commission is not responsible for any use that may be made of the information it contains.

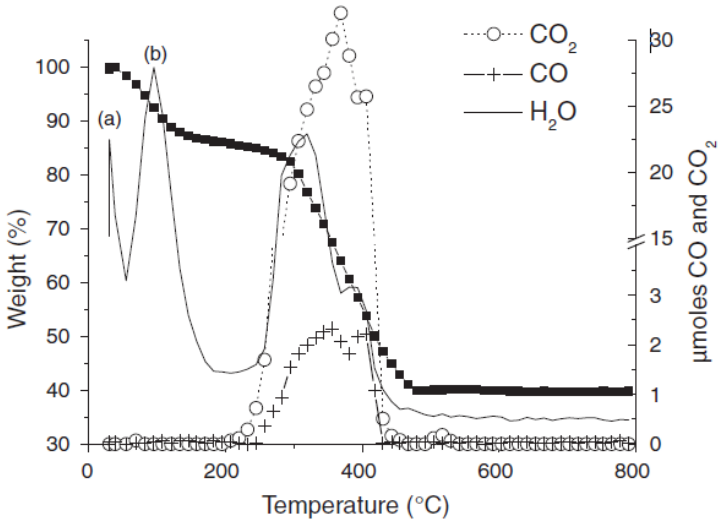

Figure 9 : TGA analysis and µlGC monitoring of H_2O, CO_2 and CO emission during the calcination of UO_2^{2+}–Am^{3+} loaded resin in air.

Degradation of carboxylic skeleton in the form of CO_2, H_2O and CO occurs between 250 °C and 480 °C in an exothermic reaction with a weight loss of 44.8%. A maximum release peak is observed at 370 °C. Experimental weight loss of 44.8% of the hydrated loaded resin, which corresponds to a 53.2 ± 0.8% weight loss of the fully dehydrated loaded resin, can be compared to the theoretical weight loss calculated form the following thermal degradation reaction:

$$R_{21}(UO_2)_9Am,(RH)_{11} \xrightarrow{+O_2,-CO_2,-CO,-H_2O} 3\,(U_3O_8) + AmO_2$$

With R standing for the ionogenic group of the resin and having a molecular weight of 75.5 g mol^{-1} [31].Experimental value of 53.2% is in fair agreement with the theoretical value of 53.0% which confirms the formulation of the loaded resin.

CHARACTERIZATION OF THE OXIDE MICROSPHERES

Loaded resin was calcined by applying the two thermal treatments exposed previously and the reduced oxide microspheres obtained were characterized.

XRD ANALYSIS.

The XRD pattern obtained from the powdered oxide microspheres is shown in **Figure 10**. It is characteristic of a single fluorite phase with a lattice parameter of 5.4511(2) Å (refined by Pattern Matching using the Fullprof Suite software [32]). This parameter is inferior to usual lattice parameter found for $U_{0.90}Am_{0.10}O_{2\pm\delta}$ compound (5.469 Å) [20, 33], and would indicate that the synthesized oxide is more oxidized than samples usually reported. The single-phased compound would suggest a homogeneous distribution of cations to be confirmed by WDX spectroscopy. Redox states of uranium and americium in the reduced compound have yet not been studied. From the literature on compounds prepared in similar conditions, americium is present as Am(III), while uranium is partially oxidized thus presenting a mixed U(IV)/(V) valence, with close Am(III) and U(V) contents [20, 26, 34, 35]. Based on the relatively low lattice parameter, a higher ratio of U(V) is expected.

This project has received funding from the EURATOM research and training programme 2014-2018 under grant agreement No 755171. The content of this deliverable reflects only the author's view. The European Commission is not responsible for any use that may be made of the information it contains.

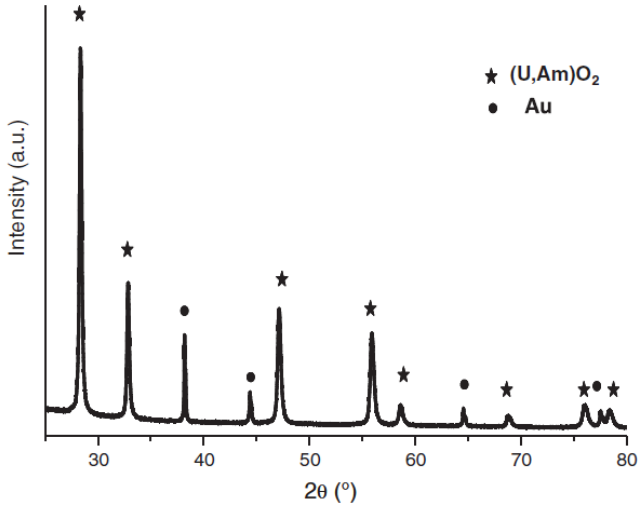

Figure 10 : XRD pattern of the oxide microsphere precursor (Au used as internal standard).

RESIDUAL CARBON CONTENT

Thermogravimetric analysis (TGA–µGC) was performed in air up to 1000 °C on the oxide precursor obtained after the two thermal treatments and results are shown in **Figure 11**. Most CO_2 gas release was recorded between 170 and 550 °C with a maximum at 275 °C corresponding to oxidation of residual carbon. A second zone was observed in the range of 925 °C and 1000 °C but at a lower extent. Total residual carbon content measured in the reduced oxide is equal to 1500 ± 100 ppm and is close to that obtained for co-converted oxalates **(see chapter on $U_{0.85}Am_{0.15}O_{2\pm\delta}$ from oxalic co-conversion route)**. As the carbon content did not preclude the densification in the latter case, carbon content in microspheres should not be a problem.
Reoxidation of the oxide $U_{0.90}Am_{0.10}O_{2\pm\delta}$ was also revealed during the experiment by weight increase.

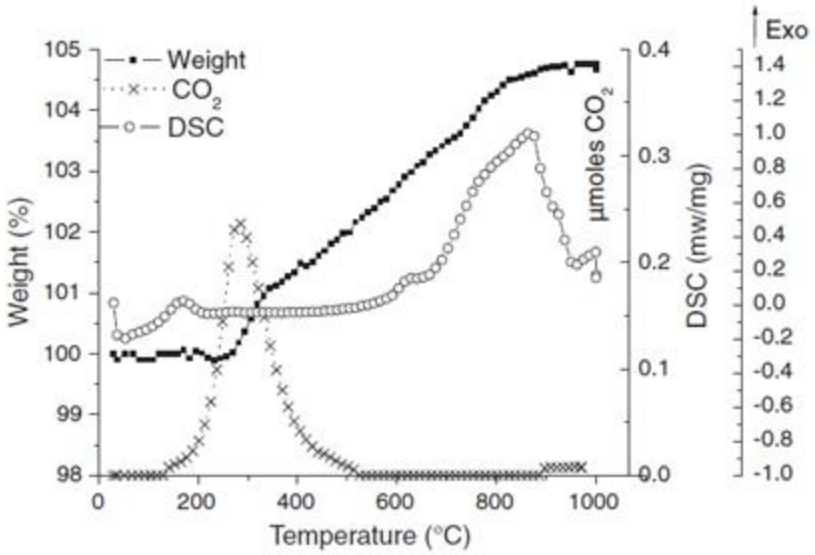

Figure 11 : TGA/DSC analysis and µGC monitoring of CO_2 emission during calcination under air of reduced $U_{0.9}Am_{0.1}O_{2\pm\delta}$ microspheres.

This project has received funding from the EURATOM research and training programme 2014-2018 under grant agreement No 755171. The content of this deliverable reflects only the author's view. The European Commission is not responsible for any use that may be made of the information it contains.

MICROSTRUCTURAL CHARACTERISTICS

SEM micrographs showing the morphology and the internal microstructure of oxide spheres are given in **Figure 12.** They prove that the spherical morphology of the resin bead is preserved during heating treatments and that the precursor microstructure is homogeneous and composed of micron-sized aggregates bounded in a large porous network. The microstructure already indicates that this material is very brittle and should be suitable for pelletization.

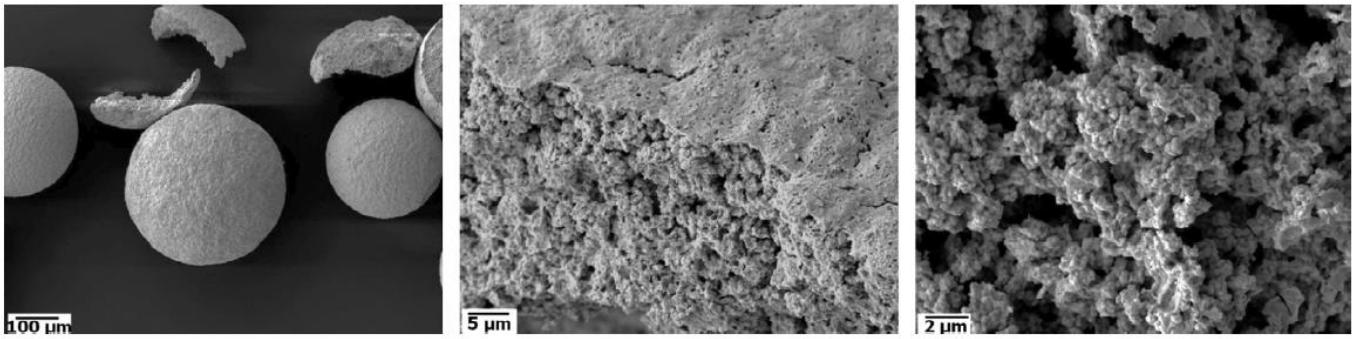

Figure 12 : FEG-SEM micrographs in secondary electron mode showing reduced oxide microsphere morphology and internal microstructure.

DENSITY.

The bulk density of oxide spheres was measured from a set of 144 microspheres. The average diameter of the spheres is 375 ± 50 µm, and the apparent density measured is of 2.7 ± 0.1 g cm^{-3}. This represents 24.0 ± 1.3% TD of the mixed oxide $U_{0.90}Am_{0.10}O_{2\pm\delta}$ calculated from the experimental refined lattice parameter obtained on reduced oxide precursors, i.e., 11.09 g cm^{-3}. This relatively low value confirms the presence of a highly porous material.

FABRICATION OF $U_{0.9}Am_{0.1}O_{2\pm\delta}$ PELLET FROM MICROSPHERES

GREEN AND SINTERED PELLETS

A mass of approximately 600 mg of oxide precursors was pressed into pellet. The green pellet obtained was sintered in a dilatometer under Ar/H_2 (4 vol.%) and the axial linear shrinkage was recorded as a function of temperature (**Figure 13**). Table 3 summarized the green and sintered pellet characteristics.

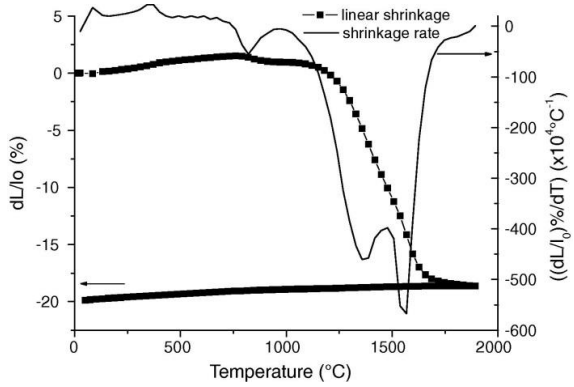

Figure 13 : Dilatometric analysis of $U_{0.9}Am_{0.1}O_2$ green pellet: axial shrinkage and shrinkage rate curves in function of temperature under a reducing atmosphere of Ar/H_2 (4 vol.%).

This project has received funding from the EURATOM research and training programme 2014-2018 under grant agreement No 755171. The content of this deliverable reflects only the author's view. The European Commission is not responsible for any use that may be made of the information it contains.

Table 3 : Green and sintered $U_{0.9}Am_{0.1}O_2$ pellet characteristics.

Pellet	Mass (g)	Height (mm) ±0.01	Diameter (mm) ±0.01	Density ($g.cm^{-3}$) ±0.05	Density (%TD) ±0.05	Porosity (%) ±0.5	Axial shrinkage ±0.5 (%)	Diametral shrinkage ±0.2 (%)	Mass loss (%)
Green	578	4.54	5.44	5.47	49.4	50.6	19.6	20.4	2.2
Sintered	565	3.65	4.33	10.51	94.9	5.1			

DILATOMETRIC ANALYSIS

Several phenomena are observed during sintering. The plots of the dilatometric curve and shrinkage rate show that a slight contraction of the pellet is first recorded at around 800°C marking the beginning of sintering. Densification slows down from 850°C till 1000°C. This phenomenon could be related to crystallization mechanisms (coherent domain growth) or to carbon removal in the form of hydrogenated carbon compounds. Linear shrinkage of the pellet accelerates again at 1000°C and the highest shrinkage rate is observed at 1570°C. This temperature is significantly lower than that observed with the UMACS process, but in the same order of magnitude as that of samples prepared from a coconverted oxalate **(see chapter on $U_{0.85}Am_{0.15}O_{2\pm\delta}$ from oxalic co-conversion route)**. Shrinkage drops off from 1750°C which indicates that higher temperature should not be necessary to reach high densities if a plateau is applied. Furthermore, axial and diametral shrinkages calculated from geometrical measurements on green and sintered pellets are respectively 19.6 ± 0.7% and 20.4 ± 0.7%, revealing an isotropic shrinkage.

CARBON CONTENT

The carbon content of the sintered pellet was measured from a pellet fragment by TGA–µGC under air and was assessed to be 100 ± 10 ppm. A large decrease of carbon content (close to 93%), initially present in the oxide precursor, was achieved during sintering. This observation proves that the carbon content of the pellet can be simply managed by heating at a higher temperature than that specified for oxide precursor synthesis and can be evacuated without any dedicated treatment.

DENSITY AND MICROSTRUCTURE

The apparent density of the sintered pellet is 94.9 ± 0.5% TD. This measurement is in accordance with FEG-SEM micrographs recorded on a fractured pellet (**Figure 14**) which reveals a dense and homogeneous microstructure composed of grains of 5–15 µm. No traces of microsphere are evidenced which would prove that the microspheres were finely crushed and mixed during compaction, thus avoiding the penalizing ‘‘blackberry’’ effect **[36]**. A few submicronic pores are homogeneously dispersed throughout the pellet and are mainly located at grain boundaries. In comparison to initial precursor microstructure characteristics, grain growth is confirmed. Those observations indicate that the last stage of sintering has been reached which is consistent with the value of the sintered density **[37]**.

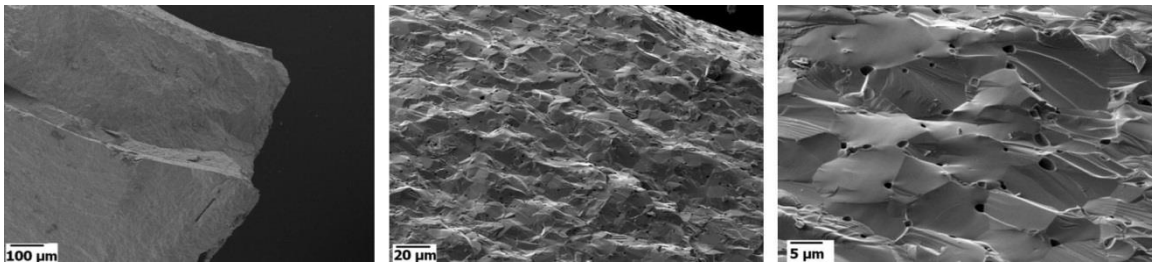

Figure 14 : FEG-SEM micrographs of $U_{0.9}Am_{0.1}O_2$ sintered pellet with a tilted SEM sample holder.

This project has received funding from the EURATOM research and training programme 2014-2018 under grant agreement No 755171. The content of this deliverable reflects only the author’s view. The European Commission is not responsible for any use that may be made of the information it contains.

STRUCTURAL ASPECTS: XRD ANALYSIS

Based on XRD pattern of a milled fragment of the sintered pellet, the oxide still exhibits a single fluorite-type structure. Refined lattice parameter is 5.4658(2)Å. This value is much higher than the lattice parameter measured on the oxide precursor (5.4511(2)Å). The most probable explanation for such a difference would be a variation of oxygen/metal ratio and, more precisely, a decrease during the sintering. This would mean that the so-called ''reduced'' microsphere were incompletely reduced compared to a pellet after sintering at 1750°C under Ar–H_2 (4 vol.%). Two reasons could explain it:

- the relatively low temperature used during the reduction thermal treatment, considering the significant reduction required (i.e., from U_3O_8 to UO_2);
- the high reactivity of the ''reduced'' microspheres after synthesis, favouring the re-oxidation of the sample during the time between the reducing heat treatment and the XRD sample preparation. A recent XRD study showed that uranium–americium mixed oxides are easily oxidized under ambient conditions [38].

CONCLUSION ON FABRICATION OF $U_{0.9}Am_{0.1}O_{2\pm\delta}$ PELLET USING CRMP PROCESS

Oxide microspheres obtained using the WAR process were suitable for pressing and a pellet with a high density of 94.9 ± 0.5% of TD was achieved after dynamic sintering under a reducing atmosphere up to 1800°C. This pellet meets the required specifications for dense pellet envisaged for Am transmutation in fast breeder reactors and proves the technical feasibility of the CRMP process for MABB application. In comparison to other fabrication process implying powder metallurgy like UMACS or co-converted route, CRMP technology presents the advantage of being a dust-free process with easily transferable materials. The green pellet obtained showed a good reactivity during sintering which would allow decreasing the common required sintering temperature (1750°C).

CONCLUSION

The main objective of all this work was to improve the way of manufacturing mixed actinide oxide pellets incorporating minor actinides for transmutation purposes either in homogeneous or heterogeneous mode, by developing more efficient processes (allowing the reduction of the sintering temperature to limit the volatilization of plutonium and minor actinides) and limiting as much as possible or even avoiding the generation of highly contaminating dust. Usually, such materials are produced using processes are based on a reactive sintering of single oxide powders and include dry steps such as milling, grinding and thermal treatments. In a first part the use of mixed oxide powder obtained via oxalic co-precipitation and thermal treatment allow the reduction of the sintering temperature due to the fact no energy spent during sintering was needed to form the oxide solid-solution. No milling or grinding was necessary, reducing the dust generation. However even using oxalic co-conversion the fabrication still implied the use of contaminant powder. To avoid it, a second process, the CRMP process, involving the handling of americium-containing precursor in the form of millimetric spheres rather than powders, was attempted with success.

This project has received funding from the EURATOM research and training programme 2014-2018 under grant agreement No 755171. The content of this deliverable reflects only the author's view. The European Commission is not responsible for any use that may be made of the information it contains.

REFERENCES

[1] F. Lebreton, D. Prieur, A. Jankowiak, M. Tribet, C. Léorier, T. Delahaye, et al., J. Nucl. Mater. 420 (2012) 213–217.

[2] M. Salvatores, G. Palmiotti, Prog. Part. Nucl. Phys. 66 (2011) 144–166.

[3] D. Prieur, A. Jankowiak, T. Delahaye, N. Herlet, P. Dehaudt, P. Blanchart, J. Nucl. Mater. 414 (2011) 503–507.

[4] T. Delahaye, F. Lebreton, D. Horlait, N. Herlet, P. Dehaudt, J. Nucl. Mater. 432 (2013) 305–312.

[5] E. Remy, S. Picart, S. Grandjean, T. Delahaye, N. Herlet, P. Allegri, et al., J. Eur. Ceram. Soc. 32 (2012) 3199–3209.

[6] J. Somers, A. Fernández, J. Am. Ceram. Soc. 88 (2005) 827–832.

[7] D. Horlait, A. Feledziak, F. Lebreton, N. Clavier, D. Prieur, N. Dacheux, T. Delahaye, J. Nucl. Mater. 441 (2013) 40–46.

[8] G. Oudinet, I. Munoz-Viallard, L. Aufore, M-J. Gotta, J.M. Becker, G. Chiarelli, R. Castelli, J. Nucl. Mater. 275 (2008) 86–94.

[9] D. Horlait, F. Lebreton, T. Delahaye, P. Blanchart, J. Am. Ceram. Soc. 1–7 (2013). http://dx.doi.org/10.1111/jace.12642.

[10] US DOE Nuclear Research and Advisory Committee and the Generation IV International Forum, A Technology Roadmap for Generation IV Nuclear Energy Systems, 2002.

[11] S. Grandjean, B. Arab-Chapelet, A.-C. Robisson, F. Abraham, Ph. Martin, J.-P.h. Dancausse, et al., J. Nucl. Mater. 385 (2009) 204–207.

[12] D. Horlait, N. Clavier, N. Dacheux, R. Cavalier, R. Podor, Mater. Res. Bull. 47 (2012) 4017–4025.

[13] B. Arab-Chapelet, S. Grandjean, G. Nowogrocki, F. Abraham, J. Alloys Compd. 444–445 (2007) 387–390.

[14] M. Vespa, M. Rini, J. Spino, T. Vitova, J. Somers, J. Nucl. Mater. 421 (2012) 80.

[15] S. Picart, H. Mokhtari, I. Ramière, I. Jobelin, IOP Conf. Ser. Mater. Sci. Eng. 9 (2010) 012025.

[16] E. Remy, S. Picart, T. Delahaye, I. Jobelin, O. Dugne, I. Bisel, P. Blanchart, A. Ayral, J. Nucl. Mater. 448 (2014) 80.

[17] S. Picart, E. Remy, T. Delahaye, Patent WO 2013/026851, 2013.

[18] K. Asakura, K. Takeuchi, J. Nucl. Mater. 348 (2006) 165–173.

[19] A. Le Bail, H. Duroy, J.L. Fourquet, Mater. Res. Bull. 23 (1988) 447–452.

[20] D. Prieur, P. Martin, A. Jankowiak, E. Gavilan, A.C. Sheinhost, N. Herlet, et al., Inorg. Chem. 50 (2011) 12437–12445.

[21] G.K. Williamson, W.H. Hall, Acta Metall. 1 (1953) 22–31.

[22] P. Pourghahramani, E. Forssberg, Int. J. Miner. Process. 79 (2006) 106–119.

[23] Z. Shao, S. Saitzek, A. Ferri, M. Rguiti, L. Dupont, P. Roussel, R. Desfeux, J. Mater. Chem. 22 (2012) 9608–9612.

[24] F. Lebreton, R.C. Belin, T. Delahaye, P. Blanchart, J. Solid State Chem. 196 (2012) 217–224.

[25] D. Horlait, F. Lebreton, T. Delahaye, N. Herlet, P. Dehaudt, Proc. Chem. 7 (2012) 485–492.

[26] D. Prieur, P. Martin, F. Lebreton, T. Delahaye, D. Banerjee, A.C. Scheinost, et al., J. Nucl. Mater. 434 (2013) 7–16.

[27] D. Prieur, A. Jankowiak, C. Leorier, N. Herlet, L. Donnet, P. Dehaudt, et al., Powder Technol. 208 (2011) 553–557.

[28] P.A. Haas, US Patent, 3.800.023, 1974.

[29] H.F. Walton, Science 138 (1962) 133.

[30] S. Picart, I. Ramie` re, H. Mokhtari, I. Jobelin, J. Phys. Chem. B 114 (2010) 11027.

[31] H. Mokhtari, Thesis, Paris XI University, Orsay; France, 2008.

[32] J. Rodríguez-Carvajal, Phys. B Condens. Matter 192 (1993) 55.

[33] D. Prieur, A. Jankowiak, D. Roudil, S. Dubois, C. Leorier, N. Herlet, P. Dehaudt, J.- P. Laval, P. Blanchart, J. Nucl. Mater. 411 (2011) 15.

[34] T. Nishi, M. Nakada, C. Suzuki, H. Shibata, Y. Okamoto, M. Akabori, M. Hirata, J. Nucl. Mater. 418 (2011) 311.

[35] K. Mayer, B. Kanellakopoulos, J. Naegele, L. Koch, J. Alloys Compd. 213–214 (1994) 456.

[36] E. Zimmer, C. Ganguly, J. Borchardt, H. Langen J. Nucl. Mater., 152 (1988), p. 169

[37] S.-J.L. KangSintering Densification, Grain Growth, and Microstructure Elsevier Butterworth-Heinemann, Amsterdam; Boston; London (2005)

[38] D. Horlait, F. Lebreton, P. Roussel, T. Delahaye Inorg. Chem., 52 (2013), p. 14196

This project has received funding from the EURATOM research and training programme 2014-2018 under grant agreement No 755171. The content of this deliverable reflects only the author's view. The European Commission is not responsible for any use that may be made of the information it contains.